A computational approach to the simulation of controlled flows by synthetic jets actuators

Michele Ferlauto[*] and Roberto Marsilio[a]

Department of Mechanical and Aerospace Engineering, Politecnico di Torino,
Corso Duca degli Abruzzi, 24, 10129, Turin, Italy

Abstract. The paper focuses on the integration of a non-linear one-dimensional model of Synthetic Jet (SJ) actuator in a well-assessed numerical simulation method for turbulent compressible flows. The computational approach is intended to the implementation of a numerical tool suited for flow control simulations with affordable CPU resources. A strong compromise is sought between the use of boundary conditions or zero-dimensional models and the full simulation of the actuator cavity, in view of long-term simulation with multiple synthetic jet actuators. The model is integrated in a multi-domain numerical procedure where the controlled flow field is simulated by a standard CFD method for compressible RANS equations, while flow inside the actuator is reduced to a one-dimensional duct flow with a moving piston. The non-linear matching between the two systems, which ensures conservation of the mass, momentum and energy is explained. The numerical method is successfully tested against three typical test cases: the jet in quiescent air, the SJ in cross flow and the flow control on the NACA0015 airfoil.

Keywords: synthetic jet; active flow control; virtual shaping

1. Introduction

Recent advances in flow control deals with Synthetic Jet (SJ) manipulators. This technology has shown widespread potential applications in aeronautics, with the aim of enhancing performances and enlarging safety margins against flow separation and stall. By low energy injections, for instance, one can modify the pressure distribution over an airfoil at high angle of attack and enhance remarkably the stall characteristics (Seifert *et al.* 1996, Smith *et al.* 1998, Gilarranz *et al.* 2005). The application of such devices has been investigated for separation control, Seifert *et al.* (1996), noise or drag reduction, Chen and Beeler (2002), lift enhancement, Smith *et al.* (1998), flow vectoring, Guo and Gary (2001) and more (see Cattafesta and Sheplak 2011, Glezer and Amitay 2002, Gad and Hak 2000, for a review). The research reveals the great potentials of flow manipulation via synthetic jets, as well as the need of tools to investigate and assess adequate control strategies. From the CFD point of view, the full simulation of the interaction between the external flow field and the flow inside the SJ manipulator requires the

---

numerical solution of unsteady, turbulent flows in time varying domains, with accurate computational schemes in both time and space.

The main problem associated with the full simulation methods is the computational cost. The numerical calculation of the cavity flow requires significant computational resources; sometime comparable with those needed to resolve the exterior flow. For geometries fitted with multiple actuators, grid requirements for the actuators could considerably exceed those of the exterior flow, and would contribute extensively to the computational cost. Space-time accurate computation requires very small time scales (actuator vibrating at some kHz) and also the code must be able to deal with very large variations of the Mach number.

For this reason, in many CFD applications of SJ the flow within the cavity in not computed and the presence of the SJ actuator is simulated by a boundary condition (BC) that imposes a periodically oscillating velocity profile at the actuator orifice (Donovan *et al.* 1998, Kral *et al.* 1997) as

$$V_n(x,t) = A(x)\sin(2\pi ft), \quad V_t(x,t) = 0, \quad \frac{\partial p}{\partial n} = -4\,\pi^2 f\rho A(x)\cos(2\pi ft) \tag{1}$$

where $A(x), f$ are the actuation amplitude and frequency, respectively, V_n, V_t are the wall-normal and tangential velocity components, ρ is density, p is pressure. Numerical experiments (Donovan *et al.* 1998, Kral *et al.* 1997) indicate that the use of *top-hat* distribution for $A(x)$ most closely matches the experimental data. The third relation in Eq. (1) expresses the boundary condition for the normal derivative of pressure at the orifice. It is derived from the momentum equation, by assuming the flow as incompressible. It must be stressed that the boundary condition introduced in Eq. (1) cancels out the mutual interaction between the SJ device and the main flow. Once the bidirectional link between the main flow and flow SJ device is broken, the information on how to recover the correct pressure level into the actuator is missed. Often, the SJ pressure level is extrapolated from the main flow interior. This practice does not preserve the conservation of mass, momentum and energy (Yamaleev *et al.* 2005), which is a crucial point during the suction phase of the cycle, where pressure is the variable that determines the influx of mass. Moreover, from a numerical point of view, an error is introduced that greatly affects the accuracy, no matter how high the order of the scheme is.

Other zero-dimensional models were proposed as an alternative for closer modeling of synthetic jet actuators and to account for additional features as well as to introduce control parameters. For instance to introduce the diaphragm dynamics (Carpenter *et al.* 2000) or to simulate a piezoelectric-driven synthetic jet actuator (Gallas *et al.* 2002). Nevertheless, even these more complicated models, based on linear governing equations, also fail in capturing flow resonances and non-linearities (Yamaleev *et al.* 2005, Rumsey *et al.* 2006), as they suffer from the same problems as the BC approach. For a more accurate review of this subject, the interested reader is referred to Yamaleev *et al.* (2005).

A way to speed up calculations is often sought case by case. In Rizzetta *et al.* (1998) the entire problem, including the flow inside the actuator, is initially computed. After several cycles of diaphragm oscillation, when the flow becomes periodic, the velocity profile across the jet exit at each time step was recorded and was used as a boundary condition in subsequent runs involving the external domain only. In Mittal *et al.* (2001) the entire actuator geometry, including the oscillating diaphragm, is simulated on a stationary Cartesian mesh.

Although the methods mentioned above have successfully been used for modeling synthetic jet actuators, several issues persist. Moreover, it must be stressed that reduced-order SJ models not considering adequately the mutual interaction with the external flow field, are not suited for cases
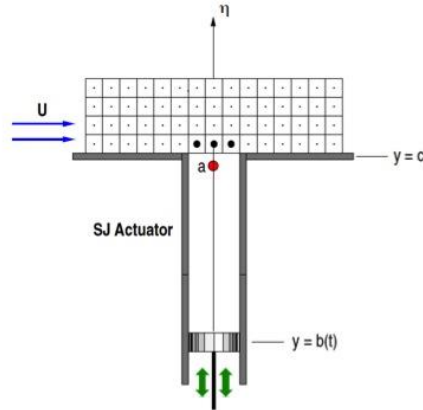
Fig. 1 A sketch of synthetic jet actuator model and its coupling with the main flow domain

where a strong coupling exists, for instance, in flow control simulations with multiple actuators in close vicinity. Conversely, for a full simulation, the resolution of the flow into the actuator cavities should require more computational resources that the external flow to be controlled (Yamaleev *et al.* 2005).

The most obvious non-linear reduced model able to ensure conservation is the Euler equations of fluid flow, as suggested by Yamaleev *et al.* (2005). They approximated the effects of the SJ actuator by Euler equations in the region far from the junction with the main flow, while the full RANS equations are adopted elsewhere. This approach is claimed to accurately predict the interaction of the synthetic jet with the external boundary layer and to resolve vortices generated in the vicinity of the actuator orifice, while reducing the computational cost. Moreover the low-dimensional actuator model: i) provides conservation of not only mass, but also momentum and energy; ii) is more efficient in terms of computational time compared with the full 2-D or 3-D numerical simulation of the actuator cavity; iii) can be used for quantitative study of the resonance characteristics of the system, since it retains some multidimensional features of the realistic actuator which are governed by the frequency and deflection of the diaphragm and the area variation and length of the quasi-1-D nozzle.

The approach retains most of the features of the full simulation with significant CPU savings, but a large number of computational points are still needed to resolve accurately the junction region. This represents a limitation for the application of the model to flow control problems, involving long time unsteady simulations with one or multiple jet actuators. Moreover, one should observe that most flow details are lost anyway at the interface between the two computational domains.

Since BC-based approaches to the simulation revealed satisfactory agreement with experimental testing in most cases, we have investigated a way to correct their lack of conservativeness by introducing an even simpler model based on the 1-D Euler equation. We was confident that the strict enforcement of mass, momentum and energy at the orifice, should give accurate results also in term of pressure.

In the present paper a non-linear model of synthetic jet actuator is proposed, based on the domain decomposition approach. The model is inspired by the work of Yamaleev *et al.* (2005) but it is does not try to approximate the flow inside the actuator but only the forcing action at the SJ

orifice, that is, at the interface with the main flow. This reduces the CPU cost to that required for the main flow computation and it is therefore more suited for flow control applications (Ferlauto and Marsilio 2009). The main flow field is simulated using standard CFD technique for compressible, turbulent flows. The flow into the actuator is modeled as the one-dimensional duct flow with a moving piston, based on the Euler equations, with the scope of generating the appropriate flow conditions at the SJ exit. The interaction at the interface of the two flowfields is evaluated by solving a Riemann problem. With little CPU expense compared to the BC approach, the proposed procedure ensures the conservation of mass, momentum and energy across the two systems and recovers their mutual inference. Simulations of some flow manipulations are discussed and compared with available data from literature.

2. Mathematical model

2.1 External flow

The mathematical model used to compute the main flow is not strictly part of the SJ model. It is described for sake of completeness, to offer the reader a coherent perspective of the numerical approach used. Obviously, the models described are those used throughout our analysis.

The main flow field is simulated using a finite volume discretization of the compressible Reynolds equations (RANS). The one-equation model of Spalart-Allmaras (S-A) (Spalart and Allmaras 1994) is used for the turbulence modeling.

The set of governing equations are written in the compact integral form

$$\frac{\partial}{\partial t}\int_v \vec{W}dv + \int_S \vec{F}_I \cdot \vec{n}dS + \int_S \vec{F}_v \cdot \vec{n}dS = \int_v \vec{H}\,dv \tag{2}$$

where v represents an arbitrary volume enclosed in a surface S. $\vec{W}$ is the hyper-vector of conservative variables, $\vec{F}_I$ and $\vec{F}_v$ are the tensors containing the inviscid and the viscous fluxes, respectively.

$$\begin{aligned}
\vec{W} &= \{\rho, \rho\vec{q}, E, \tilde{v}_t\}^T \\
\vec{F}_I &= \{\rho\vec{q}, p\bar{\bar{I}} + \rho\vec{q}\otimes\rho\vec{q}, (E+p)\vec{q}, \tilde{v}_t\vec{q}\}^T \\
\vec{F}_v &= \frac{\sqrt{\gamma M_\infty}}{Re_\infty}\left\{0, -\bar{\bar{\tau}}, -\kappa\nabla T - \bar{\bar{\tau}}\cdot\vec{q}, -\frac{v+\tilde{v}_t}{\sigma}\nabla\tilde{v}_t\right\}^T
\end{aligned} \tag{3}$$

$\vec{q} = \{u, v, w\}$ is the velocity vector, E the total energy per unit volume, M_∞ and Re_∞ are the free-stream Mach number and the Reynolds number, γ is the ratio of the specific heats and finally $\bar{\bar{I}}$ is the unit matrix. The non-homogeneous term $\vec{H}$ is due to the turbulence model:

$$\vec{H} = \left\{0,0,0, c_{b1}\tilde{S}\tilde{v}_t + \frac{c_{b2}}{\sigma}(\nabla\tilde{v}_t)^2 - c_{w1}f_w\left(\frac{\tilde{v}_t}{d}\right)^2\right\}^T \tag{4}$$

Turbulent eddy viscosity $\tilde{v}_t$ apart contains turbulence model constants and parameters. The reader is referred to Spalart and Allmaras (1994) for a full explanation of the model and constants. System (2) is non-dimensionalzed with respect to the reference length L, to free-stream density ρ_∞, temperature T_∞ and viscosity μ_∞.

The viscous stresses are written as

$$\tau_{ij} = (\mu + \mu_t) \left\{ \frac{\partial q_j}{\partial x_i} + \frac{\partial q_i}{\partial x_j} - \frac{2}{3} (\nabla \cdot \vec{q}) \delta_{ij} \right\} \tag{5}$$

where the laminar viscosity μ is computed via Sutherland's law. The turbulent viscosity $\mu_t = \rho \nu_t$ is computed through the Spalart-Allmaras one-equation turbulence model (Spalart and Allmaras 1994). The integration in time is carried out according to a 4th Runge Kutta scheme and according to an Essentially Non-Oscillatory (ENO) scheme second order accurate in both time and space. The numerical details, as well as the code validation, can be found in Ferlauto and Marsilio (2001). The numerical method has been efficiently parallelized by using OpenMP directives. The Spalart-Allmaras turbulence model has been selected after a survey of the literature on the numerical simulation of SJ flow fields by RANS solvers. When compared to $k - \epsilon$ and $k - \omega$ SST models, despite its simplicity, the S-A model has shown a closer agreement with the experimental data for the case of a synthetic jet in quiescent air (Vatsa and Turkel 2006), for the SJ in cross-flow (Rumsey *et al.* 2006) and in the evaluation of the baseline lift coefficient on the NACA0015 (Sheidahl and Klimes 1981).

2.2 Actuator flow model

Let us consider the synthetic jet device in Fig. 1 attached, for instance, beneath a flat plate on which develops a turbulent boundary layer. The actuator model consists on a duct flow generated by the moving piston. The synthetic jet is created at the actuator exit by the interaction between the external flow and the expansion/compression waves generated by the oscillating piston inside the duct. The piston is animated by a sinusoidal motion of amplitude A_p and frequency f as

$$Y(t) = A_p \sin(2\pi f t) \tag{6}$$

The strength and time scaling of the control is characterized by parameters as the reduced frequency F^+ and the momentum coefficient C_μ

$$F^+ = \frac{fx}{U_\infty}, \qquad C_\mu = \frac{d}{l} \left(\frac{U_{cl}}{U_\infty} \right)^2 \tag{7}$$

The duct is characterized by its length l and width h. For flow control applications, the SJ model aims to simulate only the interaction with the external flow, so that other details of the flow inside the actuator are neglected. In this sense the model can be seen as a conservative improvement of the BC approach.

At the interface the flow state between the two fields is evaluated by solving a Riemann problem. The numerical solver adopted for the flow in the duct integrates the one-dimensional, compressible, unsteady Euler equations in time varying domains. The actuator duct is mapped onto a normalized computational domain by the following transformation of the independent variables

$$\xi(x,t) = \frac{x - b(t)}{c(t) - b(t)}, \qquad \tau = t \tag{8}$$

where $b(t)$ and $c(t)$ are the time varying position of the left and right duct boundary, respectively. The flow governing equations are rewritten as

$$\frac{\partial}{\partial \tau} \left(\frac{U}{J} \right) + \frac{\partial}{\partial \xi} \left(\frac{U}{J} \frac{\partial \xi}{\partial t} + \frac{F(U)}{J} \frac{\partial \xi}{\partial x} \right) = 0 \tag{9}$$

where

$$U = \begin{Bmatrix} \rho \\ \rho u \\ e \end{Bmatrix} \qquad F(U) = \begin{Bmatrix} \rho u \\ p + \rho u^2 \\ (e+p)u \end{Bmatrix}, \qquad J = \frac{\partial \xi}{\partial x} \qquad (10)$$

and are integrated using a finite volume method fully compliant to that used for the external flow and having the same accuracy properties. Conventionally, the left boundary represents the piston wall, moving with velocity $b(t) = Y(t)$. The right boundary ($c(t) = 0$) is assumed as the synthetic jet slot, where a Riemann problem between the internal and the external flow is computed at each grid cell adjacent to the actuator orifice. The computed fluxes are used for the numerical integration of systems (10) and (6).

A distributed loss model could be eventually introduced to obtain more realistic velocity profile at the actuator exit. Moreover, the quasi-one dimensional formulation that allows for the duct area variation and therefore for a different actuator resonance, can be considered, as in Yamaleev *et al.* (2005). Anyway, from numerical experiments we observed that the use of variable velocity profiles is a secondary improvement, since the pressure level, which is correctly captured, plays the main role and it gives the correct estimation of the mass flow at the orifice.

2.2.1 Interface conditions between SJ actuator and external domain

The interface conditions between the main-flow and the SJ-actuator domains are treated by a characteristic- based approach. Let us consider the general case of an SJ device placed at wall and oriented at angle β with respect to the wall normal direction, as shown in Fig. 2(a). The standard approach in Godunov methods is to solve the Riemann problem at each cell interface between the external flow and the SJ domain. The suction phase and the blowing phase should be treated separately to comply with the hyperbolic nature of the flow equations. Moreover these phases are defined by observing the flow direction at the SJ outlet rather that based on the piston/diaphragm motion.

Let us start considering the blowing configuration that is when the flow exits the actuator. The wave pattern is represented in Fig. 2(b). The flow states (a) at the actuator orifice and (b) on the external flow is known. The flow states (c) and (d) are computed by using, among other, the non-linear Riemann
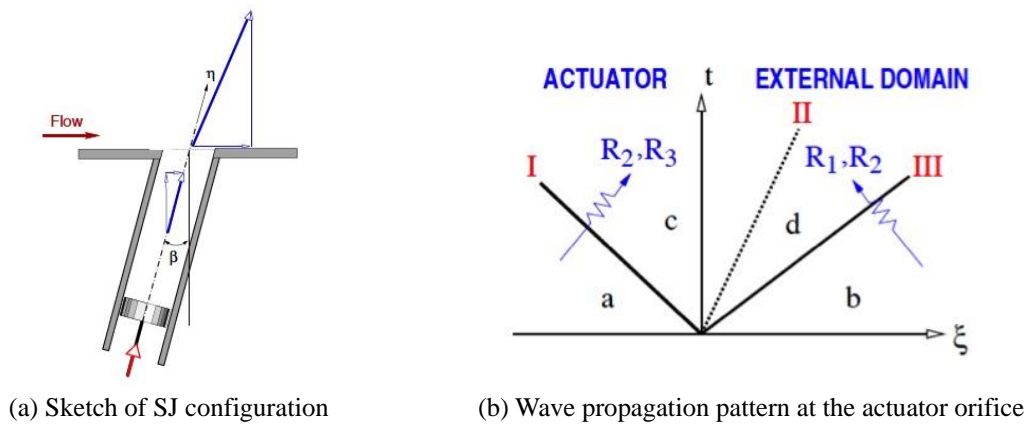

(a) Sketch of SJ configuration   (b) Wave propagation pattern at the actuator orifice

Fig. 2 SJ actuator during blowing

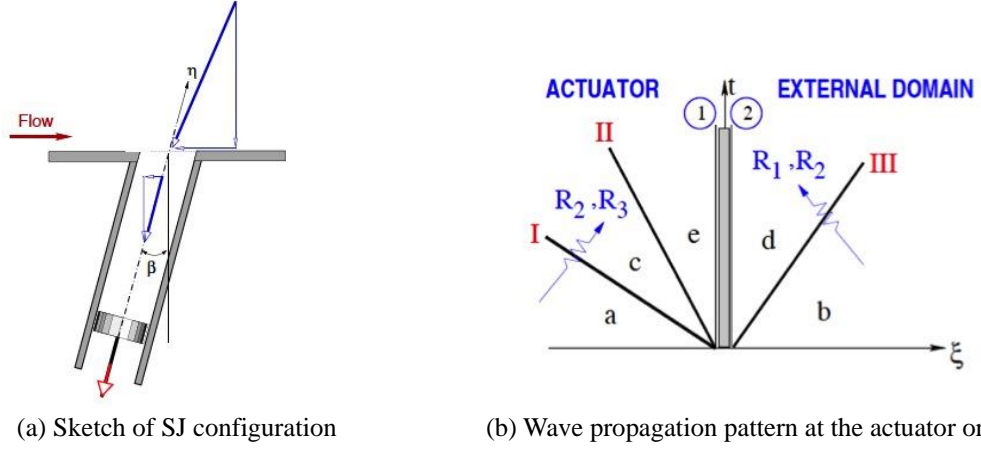(a) Sketch of SJ configuration   (b) Wave propagation pattern at the actuator orifice

Fig. 3 SJ actuator during suction

Approximated solver by Pandolfi (1983), that leads to the following closed solution

$$a_c = \frac{(R_{3a}+R_{1b})\delta}{1+\exp(\frac{S_b-S_a}{2\gamma})} \quad U_c = R_{3a} - \frac{a_c}{\delta} \quad V_c = U_c\tan(\beta) \quad S_c = S_a$$

$$a_d = a_c\exp(\frac{S_b-S_a}{2\gamma}) \qquad U_d = U_c \qquad V_d = V_b \quad S_d = S_b \tag{11}$$

where a is the speed of sound, U, V the normal and tangential velocity components in the local frame of reference and S is the entropy. The quantities

$$R_1 = \frac{a}{\delta} - U, \quad R_3 = \frac{a}{\delta} + U, \quad \delta = \frac{\gamma-1}{2} \tag{12}$$

are known as the Riemann invariants. For generic outflow configuration ($U\_c \geq 0$) the 1-D field inside the actuator and the 2-D external flow field are correctly matched, in the limit of one-dimensional splitting, according to the domain of influence and dependence of hyperbolic PDE systems.

In the suction configuration (i.e., when the flow enters the actuator), the Riemann Problem gives a back-flow solution ($U_c < 0$) and problems can arise in the splitting of tangential velocities. In fact, the assumption of a one-dimensional flow inside the actuator strictly requires $V_d = U_d\tan(\beta)$ and this can be violated if the signals impose a different tangential velocity conveyed from the external flow. Nevertheless, the solution (11) applies with good approximation, since the manipulation is often weak (e.g., virtual shaping) and the mean contribution to V_d remains negligible, as in Yamaleev *et al.* 2005).

A rigorous enforcement of the 1-D flow inside the actuator can be obtained by considering a different scheme in the suction phase, as shown in Fig. 3(b), where an actuator disk (Ferlauto and Marsilio 2006) is present at the SJ orifice, that return an axial flow in the SJ duct. Let us note that, with reference to Fig. 3(b), for the fluid states we have $(1) = (e)$ and $(2) = d$.

The Riemann problem, for the generic inflow configuration, is written by enforcing the Riemann invariants coming from the fields (a) and (b) as

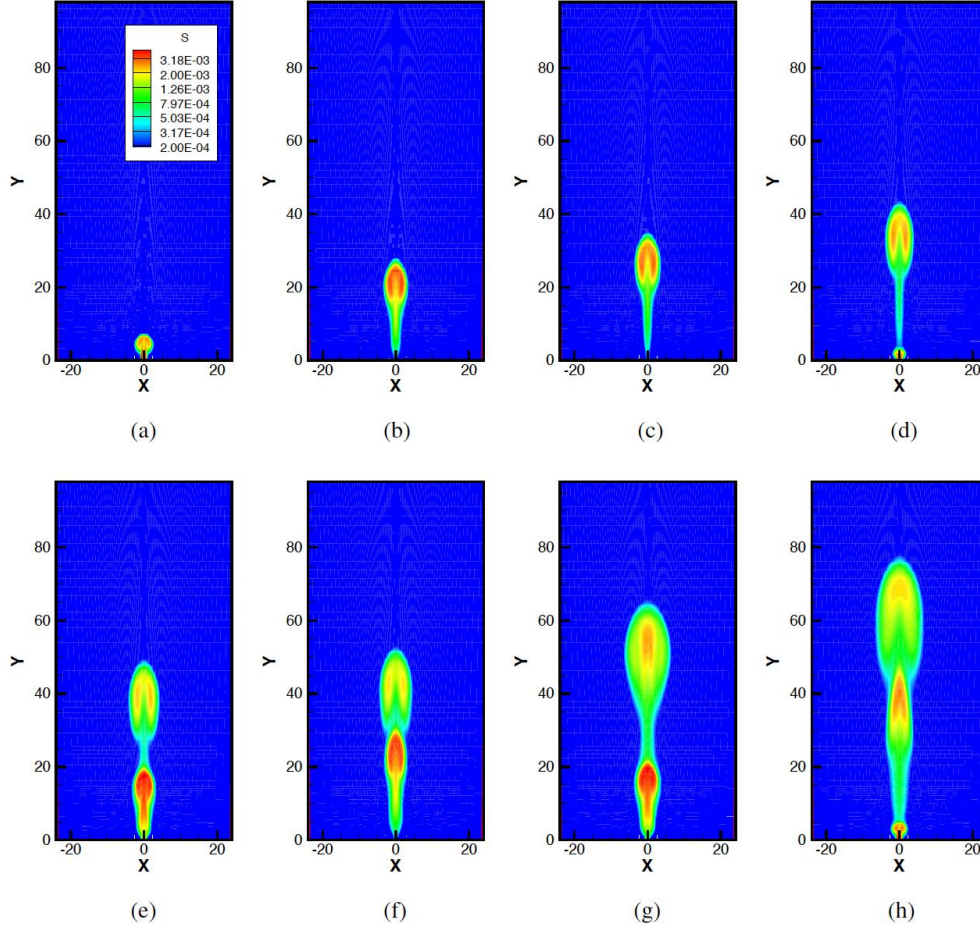$$\frac{a_c}{\delta} + U_c = R_{3a} \tag{13}$$

Fig. 4 Synthetic jet in quiescent air. The generation of the vortex flow and its evolution time for the case with f_2=40 Hz. Snapshots sequence of the entropy field at different time steps. Entropy is related to vorticity through Crocco's equation. Times scaled to the period T are: (a) t=0.25T; (b) t=0.63T; (c) t=0.83T; (d) t=1.17T; (e) t=1.46T; (f) t=1.67T; (g) t=2.5T; (h) t=3.2T

$$\frac{a_d}{\delta} - U_d = R_{1b} \tag{14}$$

then continuity is imposed across the actuator disk as

$$U_1 \left[\frac{a_1^2}{\gamma}\right]^{1/2\delta} = U_2 \left[\frac{a_2^2}{\gamma}\right]^{1/2\delta} \tag{15}$$

and the energy balance as

$$\frac{a_1^2}{2\delta} + \frac{U_1^2}{2}(1 + tan^2\beta) = \frac{a_2^2}{2\delta} + \frac{U_1^2 + V_2^2}{2} \tag{16}$$

Moreover

$$S_2 = S_1, \qquad V_1 = U_1 tan(\beta) \tag{17}$$

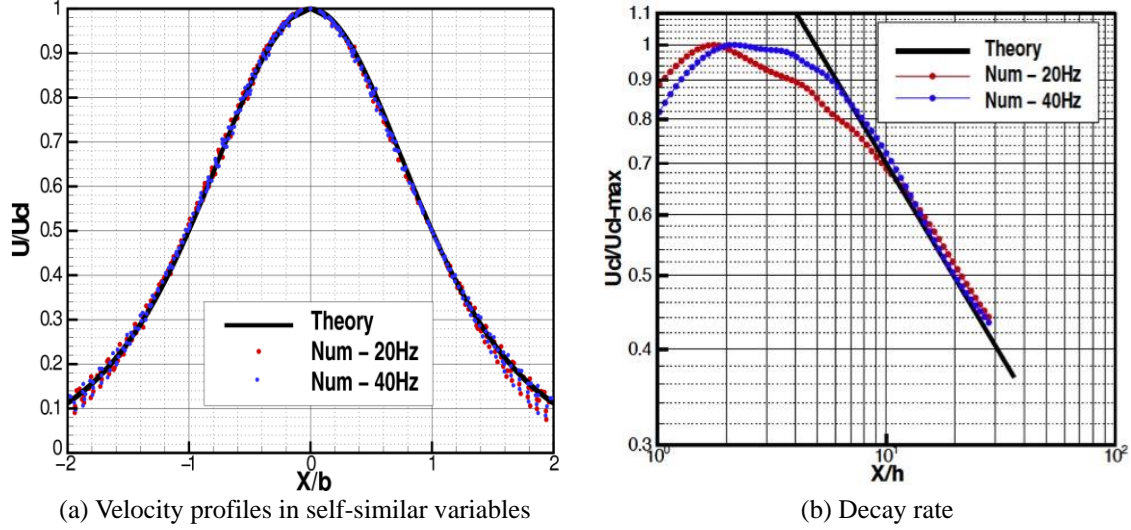(a) Velocity profiles in self-similar variables   (b) Decay rate

Fig. 5 Synthetic jet in a quiescent air: $b(y)$ is the jet width at the selected y; h is the actuator slot width

The fields are also linked by the following relation

$$
\begin{array}{ccc}
U_c = U_e = U_1 & V_c = V_a & V_d = V_b = V_2 \\
S_c = S_a = S_1 & S_d = S_b = S_2 & p_c = p_e = p_2
\end{array}
\tag{18}
$$

System (13)-(18) does not exhibit a closed form solution. It is therefore solved iteratively by the standard Newton method.

3. Numerical results

In this section some numerical experiments of flow manipulation using synthetic jet actuators are presented. The test-cases described are: the generation of a synthetic jet in a quiescent air, the interaction of SJ with a flat plate boundary layer, the flow control on NACA0015 airfoil.

### 3.1 Synthetic jet in quiescent air

The synthetic jet produced in a quiescent air and its similarities with the continuous jet have been extensively studied by Rizzetta *et al.* (1998), Vatsa and Turkel (2006), Smith and Swift (2003).

The observation that this type of actuators can reproduce the far field effects of a turbulent continuous jet was the starting point of the whole research on synthetic jets.

Present computations refer to the numerical simulation of the synthetic jet produced at $Re_h = 1710$ by a single actuator for two different forcing frequencies: $f_1 = 20\text{Hz}$ and $f_2 = 40\text{Hz}$. The Reynolds number is defined as $Re_h = (V_0 h)/\nu$ where h is the actuator slot width and

$$
V_0 = L_0 f = \frac{1}{T} \int_0^{T/2} V_{cl}(t)dt
\tag{19}
$$

Vo is the mean velocity at the SJ centerline during the blowing phase. For a sinusoidal motion the
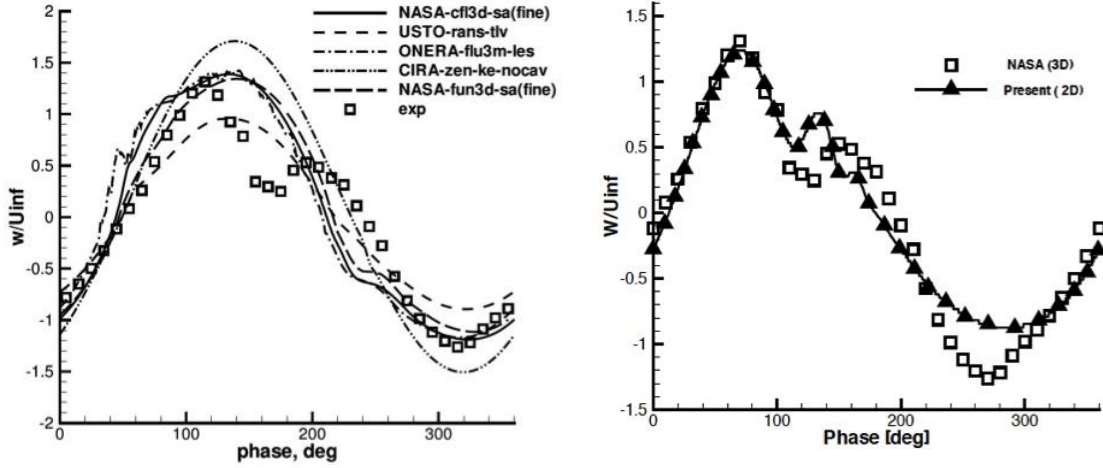
(a) Vertical velocity at the SJ orifice center for test-case 2 as reported in Rumsey *et al.* (2006)

(b) Qualitative comparison of the same experimental data with a 2-D simulation using present numerical method

Fig. 6 Synthetic jet in a cross-flow

centerline peak velocity is $V_{\max} = \pi V_0$. The parameter L_0 is the stroke length, the height of the ideal column of fluid ejected during blowing at constant velocity V_0. The numerical simulation have been performed on a 101×241 stretched grid, with 20 nodes on the SJ orifice. The grid extends for 100h in the x and 400h in the y-direction. $V_0 = 5.2$ m/s and

$$\frac{1}{F_1^+} = \left(\frac{L_0}{h}\right)_1 = 51, \qquad \frac{1}{F_2^+} = \left(\frac{L_0}{h}\right)_2 = 25.5 \tag{20}$$

The parameters of the flow simulations have been selected in the same range of Smith and Swift (2003), but the actuation frequencies are one order lower, to generate well-separated vortical structures. Nevertheless, the numerical results show that a continuous jet solution is obtained.

Snapshots of the numerical simulation of the generation and evolution of the synthetic jet are shown in Fig. 4. Starting the generation process from the ejection phase, (a) the SJ actuator pushes fluid into the external flow and a pair of counter-rotating vortices is formed at the manipulator orifice. (b) This vortex pair grows and travels in the external flow by its own induced velocity. (c) When the piston reverts its motion, it entrains external fluid into the actuator through the slot. As long as the dipole is far from the orifice, it is not effected by the motion of the entrained fluid. (d) During the subsequent ejection phase, a new dipole is formed close to the actuator orifice and (e) both vortical structures propagate into the flowfield. (f-g-h) for each cycle, at the SJ slot a new dipole is formed that interacts with the existing vortical structures and a this process, at some distance form the wall, reproduces the effects of a continuous jet. The numerical simulation is expected to converge to the self-similar solution of the continuous turbulent jet (Smith and Swift 2003, Fugal *et al.* 2005).

In Fig. 5(a) the transverse velocity profiles at different stations, obtained numerically for two actuator frequencies are compared with the theoretical solution of a turbulent two-dimensional jet. The asymptotic flow behavior is also in good agreement with the theoretical results: the decay of the centerline jet velocity reaches the theoretical rate at a distance of about 10 slot widths, as

shown in Fig. 5(b).

3.2 Synthetic jet in an external cross flow

In this section the interaction of a synthetic jet with the flat plate boundary layer is studied numerically. Our investigation focused here on a qualitative aspect of the controlled flow of Test Case 2 of NASA Workshop on CFD validation for synthetic jet (Rumsey *et al.* 2006) since the available data has put on evidence an interesting flow feature. The mentioned test case investigates, both experimentally and numerically, the three-dimensional interaction of a round synthetic jet in an external cross flow. In Fig. 6(a) the diagram of the vertical velocity during the full actuator cycle is shown, as reported in Rumsey *et al.* (2006). The experimental velocity profile shows a second positive peak that all the reported numerical simulations fail to reproduce. In our
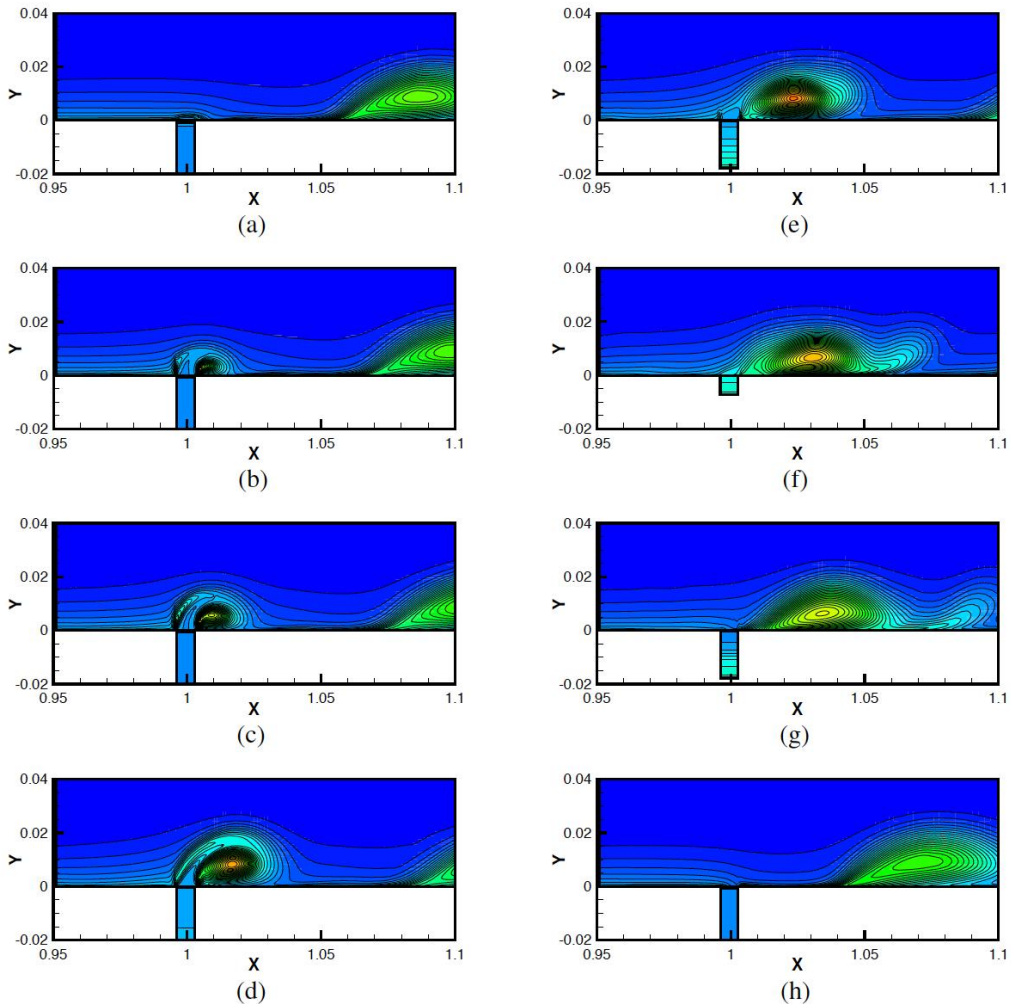

Fig. 7 Synthetic jet in a cross-flow. Snapshots of the entropy field evolution during a typical cycle of flow forcing by synthetic jets actuation
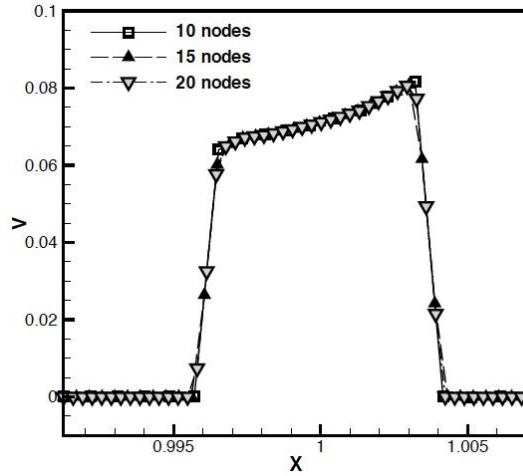
Fig. 8 Instantaneous velocity profile at the actuator exit. The curves refer to the number of nodes (10, 15 and 20) used to resolve the SJ velocity profile, for grids with 180×90, 240×120, 320×150 nodes, respectively
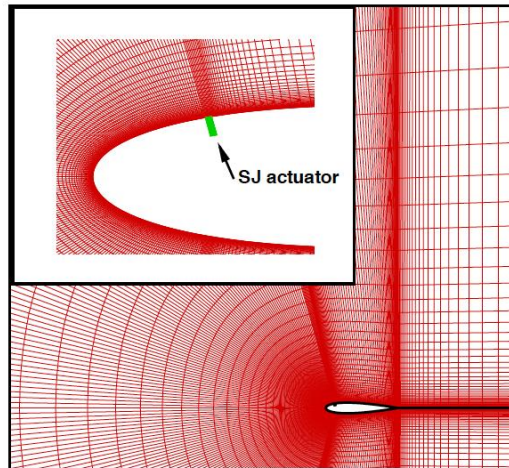

Fig. 9 A sketch of 507×121 the stretched grid around NACA0015 airfoil and on the SJ actuator

opinion, this flow feature cannot be explained as a three-dimensional effect. In fact, none of the well-assessed 3-D codes and methods used for the CFD investigation was able to capture this evident detail. We believe the secondary peak is the result of the non-linear unsteady interaction between the main flow and the flow inside the actuator. SJ models adopted in the CFD solvers failed to capture this interaction. If this interpretation is correct, the same nonlinear feature should also appear in the two-dimensional case. We were therefore motivated in studying a similar two-dimensional configuration maintaining the main adimensional parameters of Test Case 2 and fluid dynamic similarity conditions. The same reference Reynolds number $Re_{cl} = (U_\infty X_{cl})/\nu = 2.23 \cdot 10^6$ has been selected. Re_{cl} is the Reynolds number at the actuator centreline abscissa ($X_{cl} = 1$m) in the un-manipulated case. As in the experimental testing the Strouhal number is

$St = (f\,h)/U_\infty \cong 0.03$ and also the width of the SJ orifice is about one third of the boundary layer thickness.

We increase the Mach number to $M_\infty = 0.3$, that is, three times higher than the one from the experiments, to avoid slow convergence rates and loss in accuracy. As a consequence, in order to have the same Strouhal number, the actuation frequency is 450 Hz instead of 150 Hz. This choice is expected to lead to a more pronounced non-linear response of the system. Another relevant parameter of the flow control is the maximum ejection velocity V_{cl}^{max} at the SJ orifice centerline. Guidelines of Test Case 2 recommended a choice of $V_{cl}^{max} = 1.2 \div 1.3\,U_\infty$. In our model the velocity at the actuator exit is not a prescribed parameter, as we impose the piston motion. The correct value is therefore sought iteratively. The maximum ejection velocity is in fact a function of the piston forcing and of the interaction with the external flow conditions. As one can deduce from the compressible flow theory, the ejection velocity V_{max} in the blowing phase is amplified with respect to the A_p and this amplification increases with A_p strength. The peak velocity V_{max} in the suction phase remains nearly constant and close to the value of A_p. We selected the value $A_p = 0.85\,U_\infty$ as the closer approximation of the experimental profile although the ejection and suction velocities at the orifice are clearly unsymmetrical. In Fig. 6(b) the vertical velocity is plotted against the cycle phase and compared with the experimental results. Keeping in mind that this is proposed as a qualitative comparison, although obvious discrepancies between the 3-D and 2-D flow configurations, the correct behavior was recovered. The replacement of the actuator by a periodic boundary condition would instead lead to a sinusoidal evolution in time as reported in the simulations carried-out by others contributors to the NASA Workshop, as shown in of Fig. 6(a).

A snapshot sequence of the entropy field during a complete actuation cycle is shown in Fig. 7. Entropy is related to vorticity through the Crocco's equation, therefore in Fig. 7 the generation, interaction and transport of the vortical structures are also represented.

Finally, to check the consistency of our numerical solutions, a grid refinement study has been performed on three different grids: the computed velocity profiles at the SJ exit are almost superposed (see Fig. 8). Being $\delta/h > 3$, this result is not surprising since, even for the coarser grid (i.e., 180×90 with 10 nodes on the actuator width), an high number of the grid points fall inside the boundary layer.

3.3 Active flow control on NACA0015 airfoil

The flow over a NACA0015 profile, and its control, has been widely investigated in literature (Seifert *et al.* 1996, Gilarranz *et al.* 2005, Chen and Beeler 2002, Sheidahl and Klimes 1981, Rehman and Kontis 2006, Duvigneau and Visonneau 2006, Traubs *et al.* 2004, Orazi *et al.* 2011) and it represents a good candidate for a test-case and for code validation. We selected as a reference the experimental work of Gilarranz *et al.* (2005) to test the proposed model and the numerical procedure. The flow around a NACA0015 airfoil at $Re = 8.96 \cdot 10^5$ was simulated for incidence angles up to 20 degrees, with and without control via SJ.

The numerical simulations of the active stall control on the NACA0015 airfoil have been performed by following the guidelines of experimental testing of Gilarranz *et al.* (2005). The SJ actuator is placed at 12% of the airfoil chord ($X_{cl}/c = 0.12$). The forcing parameter are: $f = 60$Hz, $F^+ = 0.57$, $C_\mu = 0.005$. The computations for the uncontrolled and controlled test-cases were performed on the same 507×121 stretched mesh shown in Fig. 11. The distance between the first node and the wall has been chosen in order to have $y^+ < 1$. Tangential stretching has been

also introduced to better refine the SJ slot area, with 10 nodes along the SJ slot width. The baseline airfoil characteristic is computed first, then the control via SJ actuation is simulated and, finally, some checks on the boundary conditions and a grid sensitivity analysis are performed.

For validation purposes, a series of computations were performed to evaluate numerically the baseline flow performances, with the SJ actuator off. The results, obtained by using present flow solver, are shown in Fig. 10(a), where the numerical reconstruction of the baseline plot of lift coefficient (C_L, α) is compared with different sets of experimental data. The results obtained by
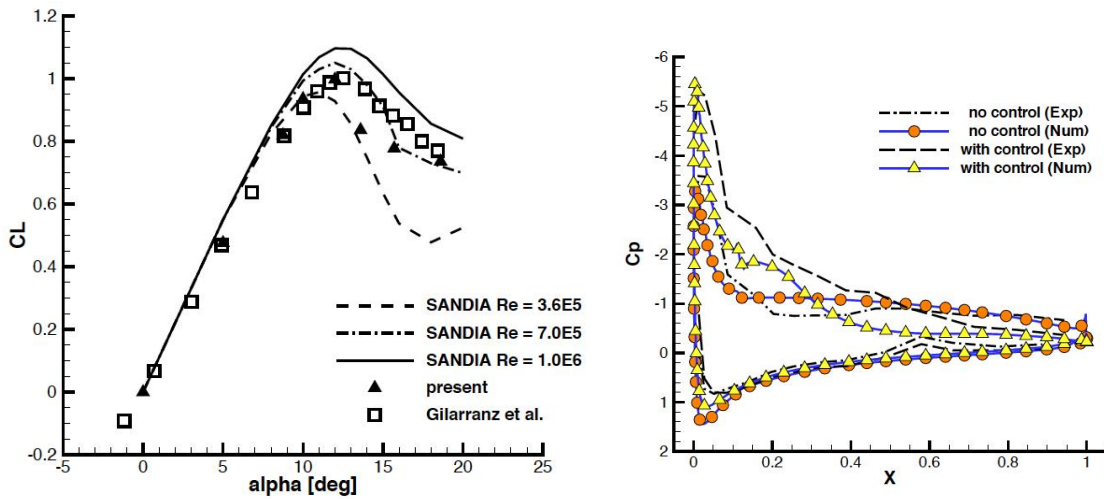
(a) Comparison of present numerical results against experimental data (Gilarranz *et al.* 2005, Sheidahl and Klimes 1981) of the baseline lift coefficient

(b) Phase averaged pressure coefficient distribution along the airfoil with and without manipulation by SJ at 15.7 of incidence

Fig. 10 NACA0012 test-case
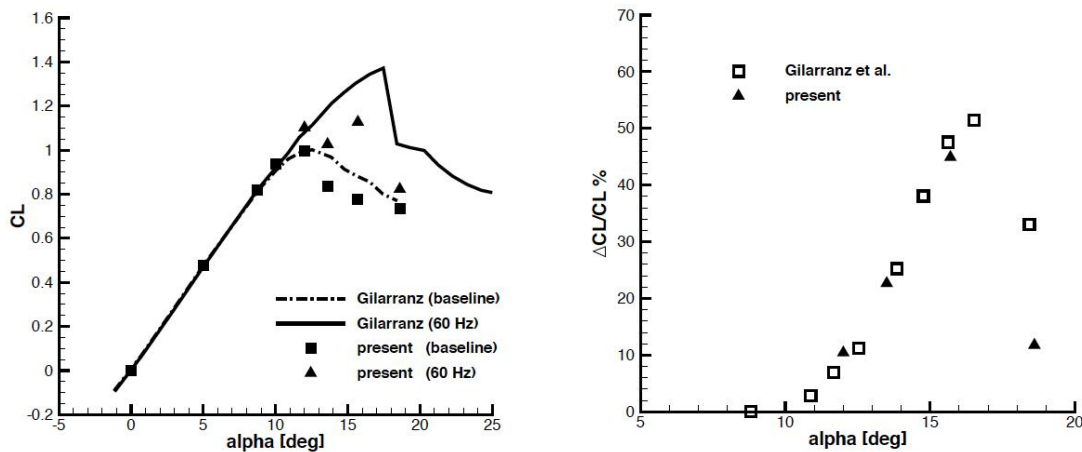
(a) Lift coefficient

(b) Lift coefficient increase, ΔC_L

Fig. 11 Active control of NACA0015 airfoil. Comparison of present numerical results with the experimental data of (Gilarranz *et al.* 2005) at 60Hz
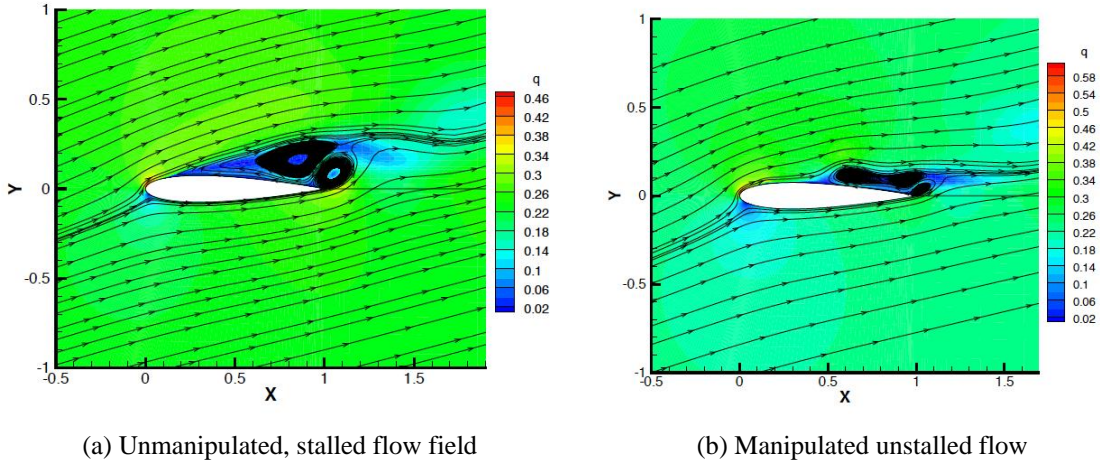
(a) Unmanipulated, stalled flow field

(b) Manipulated unstalled flow

Fig. 12 NACA0015 test-case at 15.7^0: iso-contours plot of velocity magnitude and streamlines

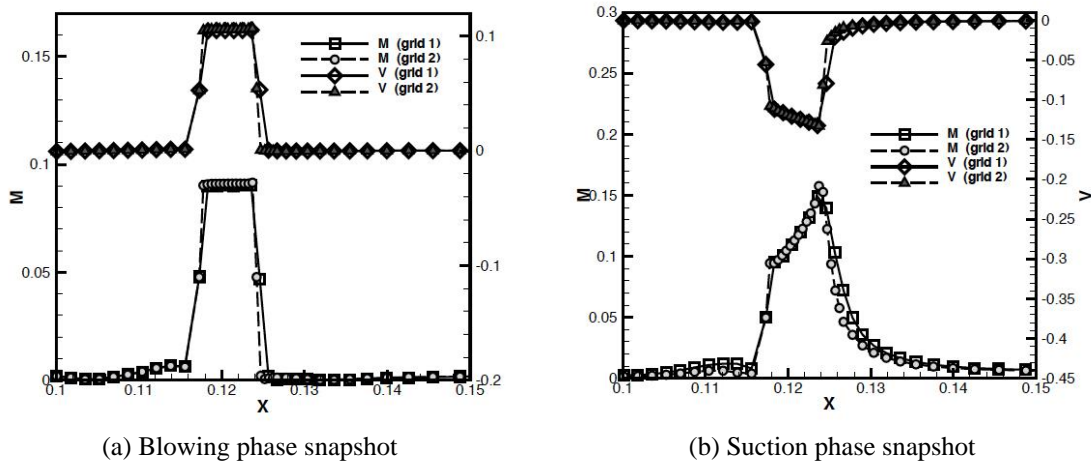(a) Blowing phase snapshot

(b) Suction phase snapshot

Fig. 13 NACA0015 test-case. Instantaneous profiles of Mach number and wall-normal velocity on the airfoil region close to SJ actuator orifice. Grid1 (507x121) and grid2 (518x121) have 10 and 20 nodes along the actuator slot width, respectively.

using the Spalart-Allmaras turbulence model are in good agreement with the experiments for a wide range of incidence, both in the pre-stall and post-stall region. The higher mismatch appears in the post-stall region, where the lift is under-predicted, with an error that remains small, within the 12%. More sophisticate turbulence models have shown higher errors in the numerical prevision of the performances of NACA0015 in post-stall conditions. Rehman and Kontis (2006) (Table 1), for instance, solving the same test-case, by using $k - \omega$ SST and $k - \varepsilon$ turbulence models have reported mean errors in the post stall region of the baseline CL curve of 30% and 72%, respectively.

Typical plots of the surface pressure coefficient C_p at $\alpha = 15.7^o$ of incidence angle, with actuation on (control) and off (with control), are shown in Fig. 10(b) where they are compared with experimental data.

The performances with active flow manipulation are presented in Fig. 11. As visible, the gap between the experimental data by Gilarranz *et al*. (2005) and the numerical simulation is slightly increased with respect to the uncontrolled case, Fig. 11(a). Nevertheless, the estimation of the relative lift increase still remains accurate. As shown in the Fig. 11(b), where the $\Delta C_L/C_L$ versus incidence is plotted, the agreement is excellent up to an incidence angle of 15.7 degrees. At the same incidence, a sketch of flowfield around the airfoil in post-stall conditions (SJ off) and the phase-averaged flow field for the unstalled, actively controlled case (SJ on) are presented in Fig. 12. In the controlled flow case, Fig. 12(b), the separation point is moved towards the airfoil trailing edge, so that a smaller separation bubble is obtained, which leads to a lift increase.

Finally the grid refinement study of the region near the actuator exit is reported. The quality of the external grid around the airfoil was tested already while computing the baseline flow. Therefore, starting from the reference grid of Fig. 9, the number of nodes along the actuator slot width was doubled by adding computational points. The two grids are then identical everywhere except in the SJ exit region. The most relevant results of these tests are summarized in Fig. 13, where the instantaneous fields computed with the two grids, having 10 and 20 nodes, respectively, on the actuator orifice, have been compared. The Figs. 13(a)-(b) show the region where some differences on the flow variable can be appreciated, that is, the region close to the actuator orifice. The Mach number distribution and the wall-normal velocity profile are plotted at suction and at a blowing instant. As visible the differences are confined to very local effects of the discretization. Streamwise propagation of the error or spurious perturbations that influence the downstream stalled/unstalled flow are not observed.

4. Conclusions

The mathematical model of a SJ actuator and its numerical implementation within a RANS code for compressible fluid flows has been presented. The model aimed to overcome conservativeness issues of other reduced order approaches and also to be suited for long-term simulation of actively controlled flows with multiple synthetic jet actuators. The significant increase of computational costs of more sophisticate modeling is avoided. The numerical method is successfully tested against three typical test-cases: the jet in quiescent air, the SJ in cross-flow and the flow control on the NACA0015 profile.

These tests reveal a good agreement with experimental data. Vortical flows characteristics have been correctly captured in the asymptotic behavior of the synthetic jet and for the case of stalled/unstalled flows on the airfoil. For the case of the boundary layer manipulation on a flat plate, it has been shown that the model reproduces the non-linear actuator response effects reported in the experimental data. The simulations of the uncontrolled and actively controlled flow fields require comparable computational resources. When the same grid is used, no appreciable differences in CPU-time have been observed for a single step of flow field evaluation, with SJ on and off. Obviously, the active flow control computations require shorter time-steps, for accuracy, and longer time integrations to lead the system to its asymptotic behavior.

References

Carpenter, P.W., Lockerby, D. and Davies, C. (2000), "Numerical simulation of the interaction of mems

actuators and boundary layers", AIAA Paper 2000-4330.

Cattafesta, L. and Sheplak, M. (2011), "Actuators for active flow control", *Ann. Rev. Fluid Mech.*, **43**, 247-272.

Chen, F. and Beeler, G. (2002), "Virtual shaping of a two dimensional naca0015 airfoil using synthetic jet actuator", AIAA Paper 2002-3273.

Donovan, J., Kral, L. and Cary, A. (1998), "Active flow control applied to an airfoil", AIAA Paper 98-0210.

Duvigneau, R. and Visonneau, M. (2006), "Optimization of a synthetic jet actuators for aerodynamic stall control", *Comput. Fluid.*, (**35**), 624–38.

Ferlauto, M. and Marsilio, R. (2001), "Computation of plug nozzle turbulent flowfields", *15th ISOABE Conference, ISABE Paper-1185*.

Ferlauto, M. and Marsilio, R. (2006), "Simulation of jet engine transient by a cfd method", *42nd AIAA Joint Propulsion Conference, AIAA Paper 2006-4968*.

Ferlauto, M. and Marsilio, R. (2009), "Synthetic jet actuator modeling for flow control applications", *Comput. Fluid Dyn.*, 573–578.

Fugal, S., Smith, B. and Spall, R. (2005), "Displacement amplitude scaling of a two-dimensional synthetic jet", *Phys. Fluid.*, (**17**), 451-60.

Gad, M. el H. (2000), *Flow control: passive, active, and reactive flow management*, Cambridge University Press.

Gallas, Q., Mathew, J., Kaysap, A., Holman, R., Nishida, T., Carrol, B., Sheplak, M. and Cattafesta, L. (2002), "Lumped element modeling of piezoelectric-driven synthetic jet actuators", AIAA Paper 2002-0125.

Gilarranz, J., Traub, L. and Rediniotis, O. (2005), "A new class of synthetic jet actuators - part ii: application to flow separation control", *J. Fluid. Eng.*, **127**(2), 377-387.

Glezer, A. and Amitay, M. (2002), "Synthetic jets", *Ann. Rev. Fluid Mech.*, **34**(1), 503-529.

Guo, D. and Gary, A. (2001), "Vectoring control of a primary jet with synthetic jets", AIAA paper 2001–0738.

Kral, L., Donovan, J., Cain, A. and Cary, A. (1997), "Numerical simulation of synthetic jet actuators", AIAA Paper 97-1824.

Mittal, R., Ramunggoon, P. and Udaykumar, H. (2001), "Interaction of a synthetic jet with a at plate boundary layer", AIAA Paper2001-2773.

Orazi, M., Lasagna, D. and Iuso, G. (2011). "Virtual shaping on naca0015 by means of a high momentum coefficient synthetic jet", *Int. J. Flow Control*, **3**(4), 255-275.

Pandolfi, M. (1983), "A contribution to the numerical prediction of unsteady flows", *AIAA J.*, **22**, 37-46.

Rehman, A. and Kontis, K. (2006), "Synthetic jet control effectiveness on stationary and pitching airfoils", *J. Aircraft*, **43**(6), 1782-1789.

Rizzetta, D., Visbal, M. and Stanek, M. (1998), "Numerical investigation of synthetic jet flowfields", AIAA Paper 98-2910.

Rumsey, C.L., Gatski, T.B., Sellers, W.L., Vasta, V.N. and Viken, S.A. (2006), "Summary of the 2004 computational fluid dynamics validation workshop on synthetic jets", *AIAA J.*, **44**(2), 194-207.

Seifert, A., Darabi, A. and Wygnanski, I. (1996), "Delay of airfoil stall by periodic excitation", *AIAA J.*, **33**(4), 691-707.

Sheidahl, R. and Klimes, P. (1981), "Aerodynamic characteristics of seven symmetrical airfoil sections through 180-degree angle of attack for use in aerodynamic analysis of vertical axis wind turbines", Sandia report SAND80-2114, UC-60.

Smith, B. and Swift, G. (2003), "A comparison between synthetic jets and continuous jets", *Exper. Fluid.*, **34**, 467-472.

Smith, D., Amitay, M., Kibens, V., Parekh, D. and Glezer, A. (1998), "Modification of lifting body aerodynamics using synthetic jet actuators", AIAA Paper 98-0209.

Spalart, P. and Allmaras, S. (1994), "A one-equation turbulence model for aerodynamic flows", *La Recherche Aerospatiale*, 5-21.

Traubs, L., Miller, A. and Rediniotis, O. (2004), "Effect of synthetic jet actuation on a ramping naca0015

airfoil", *J. Aircraft*, **41**(5), 1153-1162.

Vatsa, V. and Turkel, E. (2006), "Simulation of synthetic jets using unsteady reynolds-averaged navier-stokes equations", *AIAA J.*, **44**, 217-224.

Yamaleev, N. and Carpenter, M. (2006), "Quasi-1-d model for realistic 3-d synthetic jet actuators", *AIAA J.*, **44**(2), 208-216.

Yamaleev, N., Carpenter, M. and Ferguson, F. (2005), "Reduced-order model for efficient simulation of synthetic jet actuators", *AIAA J.*, **43**(2), 357-369.

EC